Journal of Microscopy, Vol. 233, Pt 1 2009, pp. 84–92
Received 13 March 2008; accepted 2 July 2008

A hybrid total internal reflection fluorescence and optical tweezers microscope to study cell adhesion and membrane protein dynamics of single living cells

M.I. SNIJDER-VAN AS*, B. RIEGER†, B. JOOSTEN‡, V. SUBRAMANIAM*, C.G. FIGDOR*,‡ & J.S. KANGER*
**Biophysical Engineering Group, Faculty of Science and Technology, Institute for Biomedical Technology, University of Twente, The Netherlands*
†Quantitative Imaging Group, Department of Imaging Science & Technology, Delft University of Technology, The Netherlands
‡Tumor Immunology, Nijmegen Centre for Molecular Life Sciences, Radboud University Nijmegen Medical Centre, The Netherlands

Key words. ALCAM, cell spreading, membrane protein distribution, optical tweezers, TIRF.

Summary

The dynamics of cell surface membrane proteins plays an important role in cell–cell interactions. The onset of the interaction is typically not precisely controlled by current techniques, making especially difficult the visualization of early-stage dynamics. We have developed a novel method where optical tweezers are used to trap cells and precisely control in space and time the initiation of interactions between a cell and a functionalized surface. This approach is combined with total internal reflection fluorescence microscopy to monitor dynamics of membrane bound proteins. We demonstrate an accuracy of ~2 s in determining the onset of the interaction. Furthermore, we developed a data analysis method to determine the dynamics of cell adhesion and the organization of membrane molecules at the contact area. We demonstrate and validate this approach by studying the dynamics of the green fluorescent protein tagged membrane protein activated leukocyte cell adhesion molecule expressed in K562 cells upon interaction with its ligand CD6 immobilized on a coated substrate. The measured cell spreading is in excellent agreement with existing theoretical models. Active redistribution of activated leukocyte cell adhesion molecule is observed from a clustered to a more homogenous distribution upon contact initiation. This redistribution follows exponential decay behaviour with a characteristic time of 35 s.

Correspondence to: M.I. Snijder-van As. Tel: +31 53 489 3359; fax: +31 53 489 1105; e-mail: m.i.snijder-vanas@utwente.nl

Introduction

Cell–cell interactions and interactions between cells and the extracellular matrix are essential for the functioning of all living organisms. Key mediators in these interactions are membrane proteins. Binding of these proteins to their specific ligands facilitates cell communication by initiating signalling pathways inside the cell in response to the outside world. It is becoming increasingly evident that for proper signalling not only the type, but also the spatial distribution of membrane proteins is important (Kusumi *et al.*, 2005; Cambi *et al.*, 2006). Furthermore, it appears that the distribution of membrane proteins is a dynamic parameter that can vary significantly during interactions (Grakoui *et al.*, 1999).

Cell–cell interaction and communication is of particular relevance in the adaptive immune system. Here, antigen-presenting cells, such as dendritic cells (DCs), present antigens (pathogens) to T cells to initiate an antigen-specific response (Janeway *et al.*, 2005). DCs are professional antigen-presenting cells; they capture pathogens, process them and present the pathogen-derived peptides at the cell surface to T cells (Banchereau *et al.*, 2000). Several studies have shown that for DC–T-cell interactions, the many membrane molecules involved in cell adhesion, antigen recognition and co-stimulation are ordered in a so-called immunological synapse (Monks, 1998; Grakoui *et al.*, 1999; Montoya *et al.*, 2002). The exact role in initiation or termination of this synapse for T-cell stimulation is not yet fully understood, but tightly controlled spatial organization of surface receptors has been proven to be essential (Varma *et al.*, 2006).

Various quantitative imaging techniques are available to study cell interactions and membrane dynamics.

Examples are fluorescence correlation spectroscopy, total internal reflection fluorescence (TIRF) microscopy, electron microscopy, confocal scanning laser microscopy (CSLM), fluorescence recovery after photobleaching and single particle tracking. For a detailed review of these techniques for cell biology studies see Jaiswal and Simon (2007) and Treanor and Batista (2007). Although these techniques are excellent tools to study many cellular and molecular aspects of the interactions, a major constraint in these experiments is that the interactions take place in a random fashion without precise control over the onset and position of the interaction. This hampers the study of, for example initial dynamics of the interacting proteins directly after contact, and interaction of cells at specific positions like patterned surfaces or other cells. Here we show that optical tweezers (OT) are excellent tools for spatial and temporal control of the interaction. With OT a highly focused laser beam is used to optically trap objects with a higher refractive index than their surrounding medium (Svoboda & Block, 1994; Lang & Block, 2003). We use OT to capture a living cell and to manoeuvre the cell towards the specific position of interaction. We have combined the OT with a TIRF microscope. TIRF microscopy uses an evanescent field that is generated at a glass–water interface to exclusively excite fluorophores that are in close vicinity (~200 nm) of the interface. TIRF thus allows obtaining images of membrane and near-membrane proteins with a high signal-to-background ratio (Axelrod, 2001) and is well suited to study for example cell-surface interactions.

In TIRF microscopy, an evanescent field is generated by a laser beam that undergoes total internal reflection at a glass–water interface. Total internal reflection is achieved if the angle of incidence of the laser beam is larger than the critical angle θ_c, which is defined as $\theta_c = \sin^{-1}(n_{\text{water}}/n_{\text{glass}})$, where n_{water} and n_{glass} denote the refractive index of water and glass, respectively.

The use of combined OT and evanescent wave microscopy has been reported before for force spectroscopy on small particles (Clapp *et al.*, 1999; Lang *et al.*, 2002). Recently, Kyoung *et al.* (2007) described an instrument combining OT and TIRF with fluorescence correlation spectroscopy for measuring *in vivo* cell signalling. We present here a hybrid TIRF-OT instrument to study the dynamics of the cell surface protein ALCAM (activated leukocyte cell adhesion molecule; CD166) when binding to its ligand CD6. ALCAM, consisting of five extracellular Ig domains and a short cytoplasmic tail, plays an important role in DC–T-cell interactions (Bowen *et al.*, 1995; Hassan *et al.*, 2004; Zimmerman *et al.*, 2006). The ALCAM distributions on the cell surface show strong changes upon interaction with other cells (Zimmerman *et al.*, 2006). This prompted us to study the dynamics of the redistributions of ALCAM using ALCAM-green fluorescent protein (GFP) expressing cells brought in contact with a CD6-coated surface. In addition, we describe a novel data analysis algorithm that allows quantitative measurement of the time-dependent cell spreading and ALCAM distribution.

Materials and methods

Hybrid TIRF-OT microscope

Figure 1 shows a schematic of the setup. The prism-based TIRF is constructed on a Zeiss Axiovert 135 TV microscope (Oberkochen, Germany), positioned on an optical table (Newport, Irvine, CA, USA). Laser light with a wavelength of 488 nm from an Ar^+ laser (Coherent Inc., Santa Clara, CA, USA) is guided to the setup by two optical fibres, one for TIRF illumination and one for epi-illumination. A shutter is positioned in front of the fibre input, to block illumination when no images are acquired, in order to minimize photobleaching. A water immersion objective (Leica 100x, NA 1.2, Wetzlar, Germany) is used to collect the fluorescence from the sample. Fluorescent images are recorded with an image intensified charge coupled device (CCD) camera (Pentamax 512FT, Roper Scientific, Trenton, NJ, USA), using WinSpec/32 (Roper Scientific).

An infrared (wavelength: 1064 nm) laser (Millennia IR, SpectraPhysics – Newport, Mountain View, CA, USA) is used for optical trapping. The power is set to 500 mW, sufficiently high for cell trapping, but low enough (light dose well below 340 MJ/cm^2) to prevent cell damage (Schneckenburger, 2005). A scanning mirror is used to steer the position of the trap in the *x*-*y* plane, whereas a moveable lens is used to position the trap in the *z*-direction; both are stepper motor driven by the MotionMaster2000 (Newport) and controlled by Labview software (National Instruments, Austin, TX, USA). In this way, the trap position is controlled independent of the focus of the objective. Lens f1 and f2 are used to image the scanning mirror at the back aperture of the objective lens, in order to maintain constant overfilling of the back aperture during scanning, thus ensuring a constant trapping force. The accuracy in the trap position, determined experimentally by using a trapped polystyrene bead and a tracking algorithm, is ~10 nm in the *xy*-plane and ~1 nm in the *z*-direction. Dichroic mirrors and filters are used to direct only the desired wavelengths to the specific parts of the setup.

Substrates

Microscope slides for cell-substrate interaction experiments were cleaned with 70% ethanol before coating. CD6-coated surfaces were prepared using a three-step method. First, the glass was incubated for 1 h at 37°C with 10 μg/mL goat antihuman Fc (Jackson ImmunoResearch, West Grove, PA, USA) in a buffer containing 20 mM Tris-HCl (pH 8.0), 150 mM NaCl, 1 mM $CaCl_2$, 2 mM $MgCl_2$ (TSM). After washing with TSM, the uncovered glass surface was blocked with TSM containing 1% bovine serum albumin (BSA), incubated for

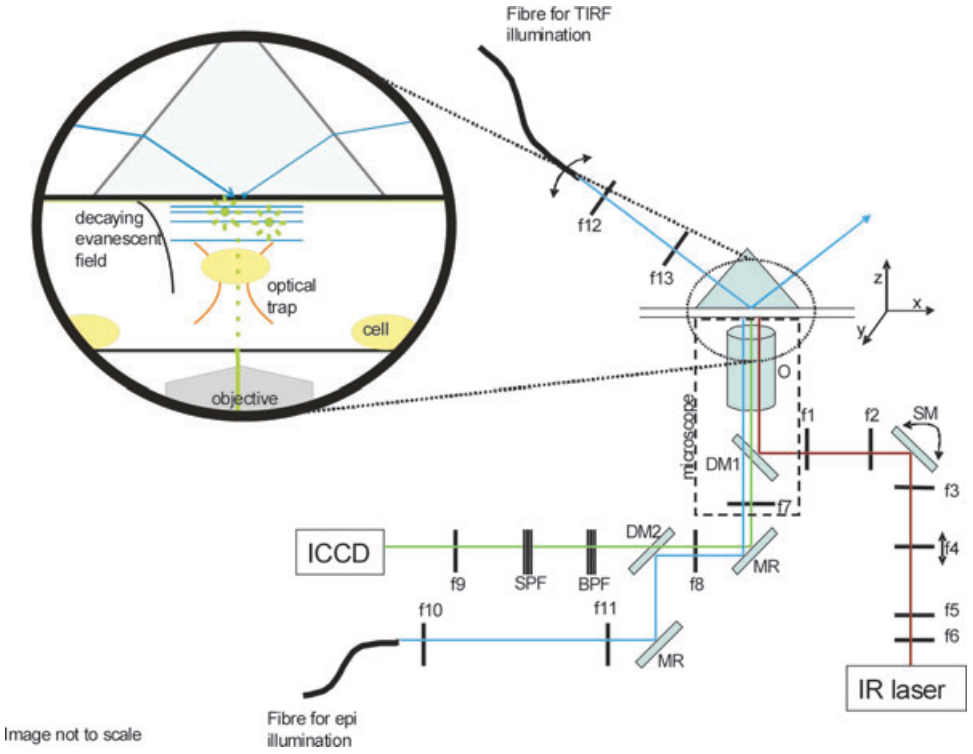

Fig. 1. Combined TIRF-OT setup: In the optical tweezers (OT) pathway (red) f1 ($f = 160$ mm), f2 ($f = 120$ mm), f3 ($f = 30$ mm) and f4 ($f = 40$ mm) are a four-lens system with a scanning mirror and a movable lens (f4) to direct the laser beam; f5 and f6 form a beam expander ($f = 100$ resp. -10 mm). The light enters the microscope through the epi-port of the microscope. DM1 (short pass 700 nm) reflects the infrared light of the OT, but transmits all other wavelengths. The light is focused by objective O. DM2 (Long pass 495 nm) is optional, and can be used for epi-illumination. The laser light for both TIRF and epi-illumination is coming through a fibre. The arm for TIRF illumination with the fibre, f12 ($f = 10$ mm) and f13 ($f = 160$ mm) is movable, to change the angle of incidence; the light is directed on a glass prism ($n = 1.52$). In the epi-path (lower blue line) f10 ($f = 20$ mm) and f11 ($f = 100$ mm) focus the light on the back of the objective. The focal length of f8 and f7 is 160 mm. In the detection path (green) a band pass filter (BPF 525/50 nm), matching the emission wavelength of the fluorophore, is used. A short pass filter (SPF 700 nm) is used to block remaining IR light. Lens f9 ($f = 400$ mm) is used to image the light on the intensified CCD camera.

30 min at 37°C, again followed by washing with TSM. Finally, the glass surface was incubated with 10 μg/mL recombinant human CD6/Fc (R&D systems, Minneapolis, MN, USA) in TSM. For checking the surface distribution, mouse anti-CD6 (BD Pharmingen, San Diego, CA, USA) was used.

BSA coated microscope cover slip glasses were prepared by incubation with a 1% BSA in TSM solution for at least 30 min. After incubation the slides were washed extensively with TSM.

The working distance of the objective limits the sample thickness from the cover slip to the side of excitation to ~70 μm. Therefore, the (coated) microscope slide at the top of the sample was separated from the (BSA coated) cover slip using two small strips of Parafilm M (Alcan Packaging, Neenah, WI, USA) as a spacer, creating a channel with a fixed depth. After briefly heating, the Parafilm firmly attached to the glass surfaces, creating a tightly fixed cuvette. Shortly before the measurement, the cell suspension was introduced into the channel by capillary forces.

Cells

K562 cells stably expressing GFP-tagged ALCAM (Nelissen *et al.*, 2000) were cultured in Iscove's modified Dulbecco's medium (Cambrex, Verviers, Belgium) containing 10% foetal calf serum (Invitrogen, Carlsbad, CA), 1% antibiotics/antimycotics (Invitrogen), and G418 (Gibco Invitrogen) as a selection medium. For checking the ALCAM expression, the mouse anti-ALCAM antibody AZN-L50 (Van Kempen *et al.*, 2001) was used.

Before measurements, the cells were washed and dissolved in serum-free, phenol-red free Iscove's modified Dulbecco's medium, at a concentration of $\sim 1 \times 10^6$ cells/mL.

Cell attachment procedure

K562 cells expressing ALCAM-GFP were used as a model system. The cell suspension was loaded in the homemade cuvette. The sample was positioned on the microscope,

equipped with a stage and objective heater in order to keep the cells at a constant temperature of 37°C. No CO_2 was provided during the experiment. The prism was placed on top of the cuvette. A drop of non-fluorescent matching oil between the prism and the cuvette prevented total internal reflection between the prism and the microscope glass. The laser light from the Ar^+ laser was directed at the glass–water interface with an angle $\theta = 63^\circ$ and illuminated a circular area of diameter 60 μm, corresponding to the field of view of the CCD camera. The average intensity of the illuminated spot was 80 W/cm^2. Next, a cell was trapped with the OT well below the microscope slide. Then, the cell was raised using the OT till the cell reaches the surface. After attachment of the cell to the CD6-coated surface, the OT were turned off.

This procedure was repeated several times to measure multiple cells. A single sample was measured for maximum of 2 h.

Data acquisition and analysis

Fluorescent images were recorded over time, by taking an image every 1, 2 or 5 second(s). The exposure time was 100 ms. The recorded fluorescence time lapse images are captured with a 12-bit CCD camera and stored in 16-bit tiff-format. Images were typical taken with a field of view of 512×512 pixels with a pixel size of 116 nm. In most cases we acquired 500–1000 time frames. The processing was done by custom written software in DIPimage (Delft University of Technology, The Netherlands, www.diplib.org), a scientific image processing toolbox for MATLAB (The MathWorks, Natick, MA, USA).

We run the software in fully automated in offline batch processing mode after image acquisition. In a first step the cell body is segmented from the background. To suppress noise we smooth the image series with a x, y, t Gaussian filter (Young & Vanvliet, 1995) (σ of 2 pixels) as a pre-processing step. This ensures in most cases the segmentation of one connected cell body. The cell, given by the total fluorescence signal, is located in each time frame by an isodata threshold (Ridler & Calvard, 1978). This method automatically finds a threshold as the weighted mean of a bimodal intensity distribution. This assumption is generally fulfilled for one bright object on a darker background. Because this approach does not use one fixed threshold for all time frames, variations in the background and/or signal do not negatively influence the quality of the segmentation. The contact area is calculated as the surface area of the cell body by counting the pixels of this cell body, which is then converted into square micrometre. Once the cell body is identified, we distinguish clusters of fluorophores (i.e. ALCAM-GFP clusters) within that area. To this end, we enhance the blob-like clusters by a tophat filter, given by a subtraction of a grey-level opening from the original image (Soille, 1999), with elliptical structuring element of size 11 pixels. By applying a new isodata threshold on the processed image within the previously identified area, we segment the clusters. From the number of clusters we compute a homogeneity measure defined by the spatial density of clusters: the number of clusters divided by the cell contact area.

Results

Development of hybrid microscopy

We have studied the interaction of ALCAM expressing cells with a CD6-coated surface, to quantify the effect of redistribution of the ALCAM on the cell membrane upon contact initiation as described by Zimmerman *et al.* (2006). For this, a hybrid microscope combining OT and TIRF is developed (Fig. 1) to allow precise control over the onset of interaction by the OT and high signal-to-background images with TIRF microscopy. There are two experimental configurations to achieve total internal reflection (Ambrose *et al.*, 1999). In objective type TIRF, the evanescent field is generated by a laser beam that passes through a high numerical aperture (NA > 1.4) objective. Alternatively, prism-based TIRF can be used, where the evanescent field is generated by a laser beam that passes through a prism at the desired angle. A requirement for the use of TIRF with OT is the use of a water immersion objective, since this allows efficient trapping of objects away from the surface of a microscope cover slip glass. However, the NA of a water immersion objective, usually ∼1.2, does not allow the use of objective type TIRF. Therefore, we applied prism-based TIRF.

Development of OT-based cell trapping and adhesion

In Fig. 2, we show the general scheme of the method developed and the obtained images. With OT a cell is trapped (Fig. 2a-I) and moved towards the CD6-coated upper surface (Fig. 2a-II) of a cuvette. Simultaneously, an evanescent field is generated at the water-surface interface that allows continuous imaging of the fluorescently labelled membrane proteins. As soon as the cell membrane is within the evanescent field, fluorescent signals are recorded (Fig. 2a-III and 2b-0). The time at which the first fluorescent signals are observed is defined as $t = 0$ s. This means that in the image a pattern can be detected with a signal-to-noise ratio >1 in a non-patterned background. We assume this corresponds with the first contact of the cell with the coated surface. Due to the limited depth of the evanescent field, no fluorescent signals from the ALCAM-GFP are detected for $t < 0$ s. The uncertainty in the contact time is determined by the speed with which the cell is moved to the glass. The OT are moved upwards in steps of 1 μm, with a speed of ∼0.6 μm/s. This causes an uncertainty in the first contact time of ∼2 s. Currently, the speed is restricted by the speed of the actuator that controls the scanning lens. The contact time uncertainty can be further decreased by increasing the speed of the scanning lens.

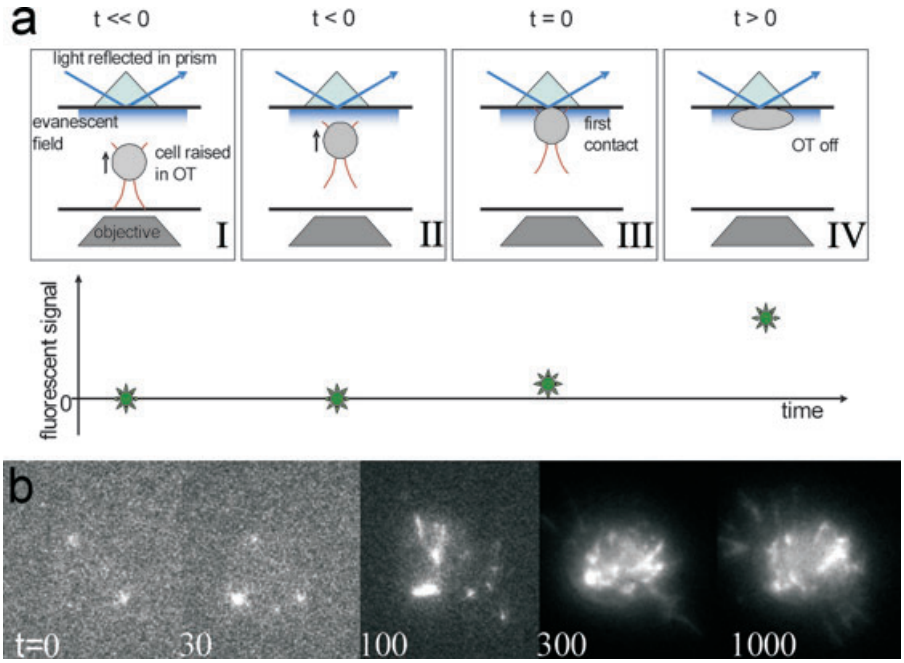

Fig. 2. OT-based cell trapping and adhesion. (a) Schematic of the method (a-I) A cell is trapped far below the upper surface of a cuvette. Prism-based TIRF is used to record fluorescence from fluorescently tagged membrane proteins. (a-II) Cell is moved upwards, but is still not in the evanescent field, so the detected fluorescent signal is zero. (a-III) Cell in first contact: $t = 0$ s, a fluorescent signal is detected. (a-IV) OT are turned off and the cell is spreading on the surface. (b) Time series of fluorescent images: K562-ALCAM-GFP in contact with a CD6-coated surface. Images are 22×22 μm and auto scaled, time is in seconds. $t = 0$ s determines point of the first contact.

When the OT are switched off, a short while after the cell is brought into contact with the surface (Fig. 2a-IV), the cell remained at the surface confirming stable contact between cell and surface. The dynamics of the cell and the membrane proteins are 'continuously' monitored by TIRF microscopy (Fig. 2b-30/100/300/1000). Control experiments with K562 cells without ALCAM-GFP expression showed no autofluorescence of the cells, so all detected light is associated with ALCAM-GFP (data not shown). Because low laser intensity was used, photobleaching appeared to be negligible. Furthermore, no fluorescence by two-photon excitation of the 1064 nm trapping laser was observed (data not shown). Cell viability before and after trapping with OT was tested using trypan blue staining, pH measurements and light microscopy to observe possible morphological changes; this revealed no damage to the cells caused by the OT (data not shown).

Quantitative analysis of contact area dynamics

The obtained images, like in Fig. 2b, are processed, as described in the materials and methods section, segmenting the image twice by isodata thresholding. A resulting image can be seen in Fig. 3, where a red line is drawn around the determined cell body and a green line around the clusters. Flow cytometry and CSLM experiments showed, by staining the ALCAM on the outside of the cell with an anti-ALCAM antibody, that almost all cells expressed ALCAM-GFP and this ALCAM-GFP is expressed at the cell membrane (data not shown). Therefore, we assume all fluorescence is from the membrane at the contact site, not from within the cell. After thresholding, the

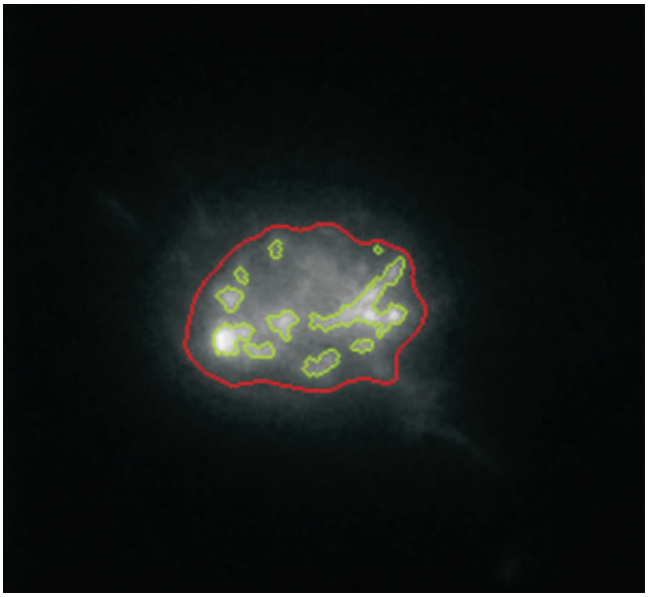

Fig. 3. Data analysis reveals the contour of both cell body (red line) and clusters (green line). Every recorded imaged is processed separately. Size of the image is ~30×30 μm.

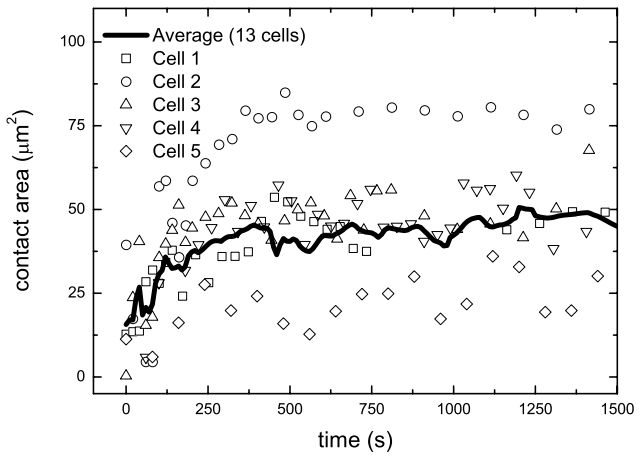

Fig. 4. Contact area over time for K562-ALCAM-GFP cells in contact with a CD6-coated surface. After a short period (∼30 s) the cell is stretching on the surface till it reaches a steady size (at ∼350 s).

data is processed further, to obtain the contact area over time and the homogeneity of the ALCAM distribution at the contact site, which are described next.

Contact area

Figure 4 shows the contact area of the cell with the microscope slide as a function of time measured for several cells in contact with a CD6-coated surface. The TIRF-OT method allows accurate determination of the time of first contact and therefore allows us to average data obtained for many different cells. As an example, Fig. 4 shows the contact area curve calculated as the average of 13 measured cells. Such averaging allows more accurate determination of the temporal evolution of relevant cell-surface contact characteristics and demonstrates one of the main advantages of combining OT with (in our case) TIRF microscopy.

Chamaraux *et al.* (2005) describe the kinetics of cell spreading. They associate stress at the margin of the contact area with actin polymerization, postulating that cell spreading is controlled by membrane-cytoskeleton attachment. Based on this, they present an analytical model for the development of the contact area over time:

$$\frac{A(t)}{A_\infty} \approx \tanh(\alpha t) \qquad (1)$$

where $A(t)$ denotes the surface contact area as a function of time t, A_∞ gives the maximum contact area for $t \to \infty$ and in which α^{-1} is a characteristic time, determined by the shear stress, Young modulus, actin polymerization speed and other cell characteristics. To account for the variation in the initial contact size, we added a constant A_0 to the expression for $A(t)$ (Eq. 1) resulting in:

$$A(t) = A_0 + (A_\infty - A_0)\tanh(\alpha t) \qquad (2)$$

To determine whether this variation in initial contact size is due to flattening of the cell on the glass caused by the pressure applied by the OT, we determined the force of the OT. The lateral escape force of the cell is ∼40 pN, which is significantly larger than the axial force active in flattening. Using a cell diameter of 15 μm and a Young's modulus for a living cell of 10 kPa (Discher *et al.*, 2005) the change in diameter of the cell caused by the OT is ∼1 nm, which can be neglected with respect to the total cell diameter. The OT thus do not influence the size of the initial contact area. The variation in the initial contact size can be understood, however, by realizing that the position of the cell with respect to the position of the optical trap is unknown. Usually, the ability to trap a cell relies on trapping a small organelle inside the cell. The position of the cell membrane with respect to the trapped organelle gives an uncertainty in the order of the diameter of the cell (∼15 μm). In addition, the membrane bound ALCAM-GFP that is already within the evanescent field, but not yet in contact with the surface, is already detected by TIRF. The influence of the extent of the evanescent field (defined as the distance from the surface at which fluorophores are still detectably exited and recognized as cell – not to be confused with the penetration depth) can be estimated assuming a spherical cell with homogenous distribution of the fluorescence at the membrane surface, using $S = \pi d(2R_{\text{cell}} - d)$; where S is the appeared contact area, d is the extent of the evanescent field and R_{cell} is the radius of the cell. For example, a cell with a radius of 7.5 μm and an extent of the evanescent field of 100 nm or 300 nm gives a calculated offset in the contact area of ∼5 or ∼14 μm², respectively, the latter is comparable to the value found experimentally. It should be noted that this offset caused by the extent of the evanescent field is most likely time dependent as the curvature of the cell membrane changes with increasing contact area. As a first approach this is not included in the model. Fitting the measured contact area curves of individual cells (Fig. 4) using Eq. 2 failed because the traces are too noisy. However, the variation between the traces of the different individual cells appears to arise mainly from the offset and final contact area and to a much lesser extent to the characteristic time $1/\alpha$. Therefore, it is reasonable to fit Eq. 2 to the averaged data. Figure 5 shows the result of fitting Eq. 2 to the averaged experimental data of Fig. 4. The model shows a good correlation with the data. This result supports the assumption that the characteristic time $1/\alpha$ does not vary much from cell to cell. From the fit we find $A_{\text{fit}} = A_\infty - A_0 = 30 \pm 0.76$ μm²; $A_0 = 13 \pm 0.74$ μm²; $\alpha = 0.005 \pm 0.0003$ s^{-1}. To compare these values with values for individual cells, we calculated the standard deviation for A_∞ and A_0 for each measured individual cell. Because fitting was not feasible, values of A_0 were obtained by averaging the contact area between time $t = 0$ s and $t = 10$ s, values of A_∞ by averaging the contact area between $t = 1000$ s and $t = 1500$ s, and values for α by a linear fit between $t = 0$ s and $t = 200$ s divided by $(A_\infty - A_0)$ [since for small t the slope of

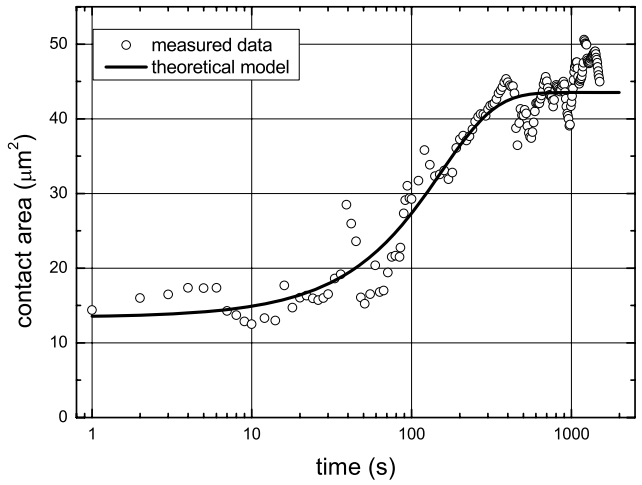

Fig. 5. Averaged (over 13 cells; circles) and fitted (solid line) contact area over time for K562-ALCAM-GFP cells in contact with a CD6-coated surface. Fit is according to Eq. 2.

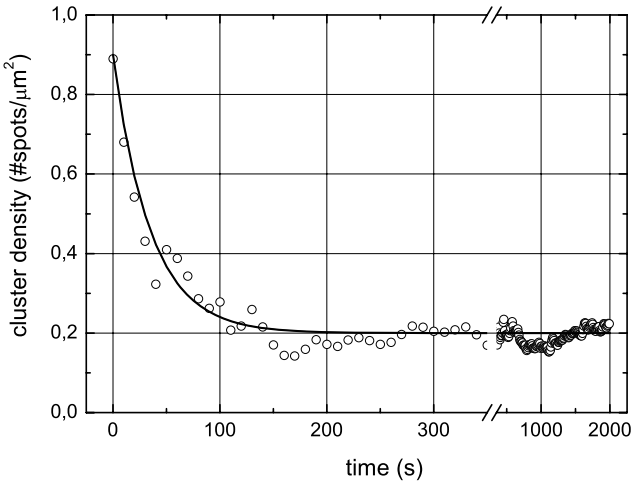

Fig. 6. Cluster density at the contact site (as a measure for ALCAM distribution), measured in number of spots per square micrometre. The circles are averaged data over 13 cells; the line is a first-order exponential decay.

Eq. 2 can be approached by $\alpha(A_\infty - A_0)$]. From this we obtained a standard deviation of A_∞ of 19 μm^2, a standard deviation of A_0 of 11 μm^2 and a standard deviation of α of 0.003 s^{-1}, confirming the large cell-to-cell variations. The mean values for $(A_\infty - A_0)$ and α, however, were similar to the ones for the averaged curve, confirming the feasibility of averaging.

Homogeneity

A more thorough analysis within the cell contact area reveals the dynamics of the distribution of the ALCAM-GFP molecules at the contact site. Within the determined cell surface, we segment the spots as described above to discriminate between clustered molecules (with a high total fluorescent intensity) and non- or less-clustered molecules (see also Fig. 3). CSLM measurements confirmed saturation and homogeneity of the CD6-coated surfaces, by staining the surface with anti-CD6 antibodies (data not shown). Therefore, we believe that the CD6 distribution is not causing the clustering at the surface. Furthermore, staining the outer cell membrane with DiI (according to the protocol of the manufacturer, Invitrogen) showed a homogenous intensity distribution indicating that the distance of the membrane to the surface is constant across the cell-surface contact area (data not shown). As a consequence the measured spatial intensity distribution of ALCAM-GFP at the contact area directly reflects the distribution of ALCAM-GFP in the contact area. The average cluster size is 0.5 μm^2 with a standard deviation of 0.4 μm^2, although also much larger clusters are observed. There was no significant change in the cluster size over time. In Fig. 6, we show the cluster density of the ALCAM-GFP distribution at the interaction site, measured as the number of clusters per square micrometre. Clearly, a fast 5-fold decrease in the number of high density spots (ALCAM clusters) per square micrometre is observed, indicating an active transition from an inhomogeneous ALCAM distribution towards a much more homogeneous distribution upon ligand binding during the first few minutes after contact initiation. Curve fitting with an exponential decay function shows a characteristic time for this transition of 35 ± 3 s. Fitting individual cell curves (when possible) revealed a mean transition time in the same order of magnitude with a standard deviation of 20 s.

Discussion and conclusion

We developed a hybrid microscopy technique by combining TIRF microscopy with OT to accurately (both in lateral position and time) initiate and monitor cell substrate interactions. We are able to determine the onset ($t = 0 \pm 2$ s) of interaction, which enables us to synchronize experiments and therefore to average the temporal dynamics of the interaction for different cells. The observed time scale for interaction in the studied system shows that this error of 2 s in the onset is an order of magnitude lower than the fasted observed dynamics ($\sim$30 s) and is thus acceptable. Therefore, the addition of OT to control the onset enables the determination of interaction dynamics with improved accuracy. We observed an offset in the contact area of 15 μm^2 (see Fig. 5). The offset was explained by both the extent of the evanescent field and the position of the cell with respect the focus of the OT. In order to reduce this offset, the penetration depth of the evanescent field could be reduced by increasing the angle of incidence θ . It should be noted, however, that beside the penetration depth of the evanescent field also the sensitivity of the fluorescence detection and the threshold in the data analysis procedure are contributing to the extent of the evanescent field. Furthermore, a rigorous

data analysis method was developed for quantitative image processing. Key parameters like contact area and cluster density of membrane proteins were determined. The method was applied to measuring interactions of K562-ALCAM-GFP cells with CD6-coated surfaces. In the quantitative analysis the assumption was made that binding of the cell to the CD6-coated surface is only mediated by ALCAM–CD6 interaction. Therefore, the cell was regarded to be in contact with the surface only at those positions where ALCAM-GFP was observed.

To quantify the observed cell spreading and redistribution process, we fitted the averaged curves with a model predicted in literature (Chamaraux *et al.*, 2005) and an exponential decay. Variables of the method influencing the variation between individual cell traces are laser power, penetration depth of the evanescent field and signal-to-background ratios. Since these values are kept constant over the experiments, these will not dramatically influence the result. By contrast to this, however, the expression level and pattern of ALCAM-GFP on the cell membrane vary for different cells. Although it is not possible to perform several experiments on the same cell to validate this, we assume based on the aforementioned arguments that cell-to-cell variations are the main cause of the variations in individual traces. Besides that, fitting individual curves with the models appeared to be difficult, because of the 'noisy' traces of these curves. This directly shows one of the main advantages of the described method, namely: to be able to average the data over different cells because $t = 0$ s is well defined. This enables fitting the data and therefore quantifying the observed processes, which would otherwise be difficult. The values obtained for cell spreading using the analysis method developed in this work were in good agreement with existing models (Chamaraux *et al.*, 2005). Furthermore, the redistribution of the ALCAM-GFP indicates an active process starting upon interaction with the CD6 surface. As can be seen comparing Figs 5 and 6, the redistribution of ALCAM (characteristic time $\sim$35 s) is significantly faster than the cell spreading [characteristic time ($=1/\alpha$) $\sim$330 s]. Therefore, it can be concluded that the increase in homogeneity is not a direct consequence of the increase in cell contact area. The average mean intensity within the cell contact area shows no significant change over time, indicating no active recruitment of more ALCAM-GFP molecules to the contact area takes place. Elucidation of the details of the mechanisms (redistribution, recruitment, or combinations of both) will require, for example experiments where the cytoskeleton is influenced. Most likely, both cell spreading and active redistribution of ALCAM on the cell surface are dictated by actin cytoskeleton dynamics since ALCAM-mediated adhesion is regulated through the actin cytoskeleton (Nelissen *et al.*, 2000) and ALCAM can bind to β-actin (Te Riet *et al.*, 2007).

All experiments shown here are performed on a saturated CD6-coated surface. The final concentration might therefore be different from that found on CD6 expressing cells. Additionally, it should be noted that CD6 molecules on the substrate are immobile by contrast to membrane bound CD6. Obviously, these two constraints hamper the biological interpretation of the current data. To overcome these limitations we are currently adapting our method for the study of cell–cell interactions. Since TIRF might be difficult for studying cell–cell interactions, as a result of the thickness of the cell adhering to the glass, alternative fluorescent detection schemes could be applied in combination with OT. For example, if processes are studied in which fast dynamics or high depth resolution (the advantages of TIRF) is less important, CSLM can be an option.

The method developed here is, however, not limited to the study of membrane protein dynamics. The current method is suitable for studying many near-membrane processes such as near-membrane cytoskeleton dynamics, signalling, but also processes that involve dynamics of the membrane itself like the forming of podosomes. All these processes can be studied systematically in cells interacting with other cells or with e.g. structured surfaces or bi-layers (e.g. mimicking the molecules of the immunological synapse).

The advantage of combining OT with (TIRF) microscopy over simple settling down of the cells on a surface, lies in the spatial and temporal control that is enabled by using OT. OT enable the selection of cells exhibiting specific properties (e.g. bright fluorescence), and precise control of the position of the interaction (e.g. at a specific place on a patterned surface) to enable optimal imaging conditions and interaction with the surface. In particular if one is interested in fast dynamics of membrane molecules, it is essential to choose a limited field of view, so that the number of pixels per image that need to be read out from the CCD camera can be kept to a minimum. However, this approach is only feasible if the cell-surface interaction takes place precisely within this small field of view, a condition that can be readily achieved using the approach described here. Alternative methods for temporal control are the use of micropipettes or cantilevers. However, those methods all rely on the previous attachment of the cell to either the micropipette or the cantilever, which may already induce a reaction of the cell. These approaches contrast with OT, where the cell can be brought into contact without physically touching the cell; after contact initiation, the OT can be easily turned off. We conclude that the combination of TIRF with OT-based cell manipulation provides a novel and powerful tool to yield precisely timed information on cell-substrate interactions. The unique ability to control the exact time and position of the interaction is a versatile approach in cell biology and immunology.

Acknowledgements

This work was supported by the foundation for Earth and Life Sciences (ALW), which is subsidized by the Netherlands Organization for Scientific Research (NWO).

References

Ambrose, W.P., Goodwin, P.M. & Nolan, J.P. (1999) Single-molecule detection with total internal reflection excitation: Comparing signal-to-background and total signals in different geometries. *Cytometry* **36**, 224–231.

Axelrod, D. (2001) Total internal reflection fluorescence microscopy in cell biology. *Traffic* **2**, 764–774.

Banchereau, J., Briere, F., Caux, C. *et al.* (2000) Immunobiology of dendritic cells. *Annu. Rev. Immunol.* **18**, 767–811.

Bowen, M.A., Patel, D.D., Li, X. *et al.* (1995) Cloning, mapping, and characterization of activated leukocyte-cell adhesion molecule (ALCAM), a CD6 ligand. *J. Exp. Med.* **181**, 2213–2220.

Cambi, A., Joosten, B., Koopman, M. *et al.* (2006) Organization of the integrin LFA-1 in nanoclusters regulates its activity. *Mol. Biol. Cell* **17**, 4270–4281.

Chamaraux, F., Fache, S., Bruckert, F. & Fourcade, B. (2005) Kinetics of cell spreading. *Phys. Rev. Lett.* **94**, 1581021–1581024.

Clapp, A.R., Ruta, A.G. & Dickinson, R.B. (1999) Three-dimensional optical trapping and evanescent wave light scattering for direct measurement of long range forces between a colloidal particle and a surface. *Rev. Sci. Instrum.* **70**, 2627–2636.

Discher, D.E., Janmey, P. & Wang, Y.L. (2005) Tissue cells feel and respond to the stiffness of their substrate. *Science* **310**, 1139–1143.

Grakoui, A., Bromley, S.K., Sumen, C., Davis, M.M., Shaw, A.S., Allen, P.M. & Dustin, M.L. (1999) The immunological synapse: A molecular machine controlling T cell activation. *Science* **285**, 221–227.

Hassan, N.J., Barclay, A.N. & Brown, M.H. (2004) Optimal T cell activation requires the engagement of CD6 and CD166. *Eur. J. Immunol.* **34**, 930–940.

Jaiswal, J.K. & Simon, S.M. (2007) Imaging single events at the cell membrane. *Nat. Chem. Biol.* **3**, 92–98.

Janeway, C.A., Travers, P., Walpost, M. & Shlomchik, M.J. (2005) *Immunobiology: the Immune System in Health and Disease*. 6th edn. Garland Science Publishing, NY.

Kusumi, A., Ike, H., Nakada, C., Murase, K. & Fujiwara, T. (2005) Single-molecule tracking of membrane molecules: plasma membrane compartmentalization and dynamic assembly of raft-philic signaling molecules. *Semin Immunol* **17**, 3–21.

Kyoung, M., Karunwi, K. & Sheets, E.D. (2007) A versatile multimode microscope to probe and manipulate nanoparticles and biomolecules. *J Microsc* **225**, 137–146.

Lang, M.J. & Block, S.M. (2003) Resource letter: LBOT-1: Laser-based optical tweezers. *Am. J. Phys.* **71**, 201–215.

Lang, M.J., Asbury, C.L., Shaevitz, J.W. & Block, S.M. (2002) An automated two-dimensional optical force clamp for single molecule studies. *Biophys. J.* **83**, 491–501.

Monks, C.R.F., Freiberg, B.A., Kupfer, H., Sciaky, N. & Kupfer, A. (1998) Three-dimensional segregation of supramolecular activation clusters in T cells. *Nature* **395**, 82–86.

Montoya, M.C., Sancho, D., Vicente-Manzanares, M. & Sanchez-Madrid, F. (2002) Cell adhesion and polarity during immune interactions. *Immunol. Rev.* **186**, 68–82.

Nelissen, J.M.D.T., Peters, I.M., de Grooth, B.G., van Kooyk, Y. & Figdor, C.G. (2000) Dynamic regulation of activated leukocyte cell adhesion molecule-mediated homotypic cell adhesion through the actin cytoskeleton. *Mol. Biol. Cell* **11**, 2057–2068.

Ridler, T.W. & Calvard, S. (1978) Picture thresholding using an iterative selection method. *IEEE Trans. Syst. Man Cybernet.* **8**, 630–632.

Schneckenburger, H. (2005) Total internal reflection fluorescence microscopy: technical innovations and novel applications. *Curr. Opin. Biotechnol.* **16**, 13–18.

Soille, P. (1999) *Morphological Image Analysis. Principles and Applications*. Springer-Verlag, Berlin.

Svoboda, K. & Block, S.M. (1994) Biological Applications of Optical Forces. *Annu. Rev. Biophys. Biomol. Struct.* **23**, 247–285.

Te Riet, J., Zimmerman, A.W., Cambi, A. *et al.* (2007) Distinct kinetic and mechanical properties govern ALCAM-mediated interactions as shown by single-molecule force spectroscopy. *J Cell Sci.* **120**, 3965–3976.

Treanor, B. & Batista, F.D. (2007) Mechanistic insight into lymphocyte activation through quantitative imaging and theoretical modelling. *Curr. Opin. Immunol.* **19**, 476–483.

van Kempen, L., Nelissen, J., Degen, W.G.J. *et al.* (2001) Molecular basis for the hemophilic activated leukocyte cell adhesion molecule (ALCAM)-ALCAM interaction. *J. Biol. Chem.* **276**, 25783–25790.

Varma, R., Campi, G., Yokosuka, T., Saito, T. & Dustin, M.L. (2006) T cell receptor-proximal signals are sustained in peripheral microclusters and terminated in the central supramolecular activation cluster. *Immunity* **25**, 117–127.

Young, I.T. & Vanvliet, L.J. (1995) Recursive Implementation of the Gaussian filter. *Signal Process.* **44**, 139–151.

Zimmerman, A.W., Joosten, B., Torensma, R., Parnes, J.R., van Leeuwen, F.N. & Figdor, C.G. (2006) Long-term engagement of CD6 and ALCAM is essential for T-cell proliferation induced by dendritic cells. *Blood* **107**, 3212–3220.

